NMR Images of Proton Residual Dipolar Coupling from Strained Elastomers

M. Schneider, D. E. Demco, and B. Blümich*

Institut für Technische Chemie und Makromolekulare Chemie, Rheinisch-Westfälische Technische Hochschule, Worringerweg 1, D-52056 Aachen, Germany

Received November 20, 2000

ABSTRACT: Proton residual dipolar couplings of elastomer chains were used to generate contrast in NMR images of stretched elastomers. Dipolar contrast filters are discussed on the basis of dipolar encoded longitudinal magnetization as well as double-quantum and triple-quantum coherences. The associated contrast filter parameters were investigated by measurements of the line width in ^{1}H multiple-quantum filtered NMR spectra, the dipolar encoded longitudinal magnetization decay curves, and the double-quantum and triple-quantum buildup curves vs the extension ratio for a natural rubber band. Together with stress−strain measurements these results allow for correlation of ^{1}H residual dipolar couplings with stress values in stretched natural rubber. Two-dimensional ^{1}H maps of stress distributions are presented for a strained natural rubber band with a cut on one side based on dipolar encoded longitudinal magnetization and double-quantum contrast filters. Parameter maps of the stress distribution are shown following calibration with a sample from synthetic poly(isoprene). The advantages as well as the limitations of the ^{1}H NMR images as compared to ^{2}H images of deuterated oligomers incorporated in elastomers are also discussed.

Introduction

In recent years the potential of magnetic resonance imaging[1−3] in addressing problems in a wide area of different fields, such as material and polymer science, petrochemical research, plant science, and agriculture, has been realized.[4−6] Molecular characteristics can be explored with NMR methods, and the resulting NMR parameters can be used for contrast in NMR images.[7−9] Especially, for the important class of materials represented by elastomers, knowledge about segmental orientation and polymer chain dynamics is essential for understanding their macroscopic properties.[10] Diverse applications of NMR imaging in elastomers have appeared in the literature.[11] Topics addressed are phase separation,[12] selective determination of component distribution in multicomponent systems,[13] aging,[12,14,15] biodegradation,[16] water uptake,[17,18] morphology and defect distribution,[19,20] filler distribution,[21] homogeneity of cross-link density,[22−24] and stress-induced effects.[25−28]

Recently, spectroscopic ^{2}H NMR imaging and double-quantum (DQ) filtering have been compared by mapping local strain distributions in stretched elastomers.[27,28] The first method is able to give information about the local strain but requires an additional frequency dimension for spectroscopic resolution. The second approach generates NMR images in short time, but the resultant image is only a parameter-weighted image of the residual quadrupole coupling with the spin density and the transverse relaxation rate. The results show[27,28] that DQ filtering of the ^{2}H NMR signal is more sensitive for the detection of small anisotropies than spectroscopic imaging. Moreover, the ^{2}H parameter maps were compared to images of stress distributions that were simulated by finite element matrix calculation.[27]

Proton multiple-quantum (MQ) coherences, especially DQ coherences, have been explored for the investigation of residual dipolar couplings in elastomers like poly(styrene-*co*-butadiene)[29] and poly(isoprene).[30,31] When measured selectively for a given chemical structure these dipolar couplings can be correlated with the cross-link density distribution. Moreover, contrast filters for NMR imaging of residual ^{1}H dipolar couplings of elastomers were introduced on the basis of dipolar encoded longitudinal magnetization (LM) as well as double-quantum and triple-quantum (TQ) coherences.[31] Two-dimensional parameter maps were reported representing the space distribution of ^{1}H residual dipolar couplings in a phantom made of poly(isoprene) with different cross-link densities.[31] Filtered images from dipolar encoded LM and TQ show the highest resolution and contrast, respectively. Furthermore, proton as well as deuterium DQ-filtered NMR imaging has been applied to map molecular order in biological tissues.[32,33]

In this paper, we introduce ^{1}H residual dipolar NMR filters based on dipolar encoded LM, DQ, and TQ coherences for stretched elastomers. The effect of uniaxial stress on a natural rubber band is investigated for dipolar encoded LM decay curves, DQ, and TQ buildup curves as well as for the line width of spin multipole (LM, DQ, and TQ) filtered ^{1}H NMR spectra. These quantities are needed for the adjustment of the dipolar filters used for obtaining ^{1}H parameter maps of stress in strained elastomer bands made of natural rubber. The advantages as well as the limitations of this approach compared to the ^{2}H NMR imaging of stress in strained elastomers are also discussed.

Experimental Section

A. Samples. We have investigated commercially available elastic bands made from natural rubber (NR). The reference elastomer system used for calibration of stress parameter images is based on synthetic 1,4-*cis*-poly(isoprene) (PI). According to the specifications of the manufacturer, this elastomer has a molecular weight M_w = 952 110 g/mol and a molecular weight distribution M_w/M_n = 4.35. The repetition units are 97.5% *cis*-1,4-isoprene and 2.5% 3,4-isoprene. The glass transition temperature T_g is about 210 K. Cross-linking

* To whom correspondence should be addressed.

10.1021/ma001983n CCC: $20.00
Published on Web 05/03/2001

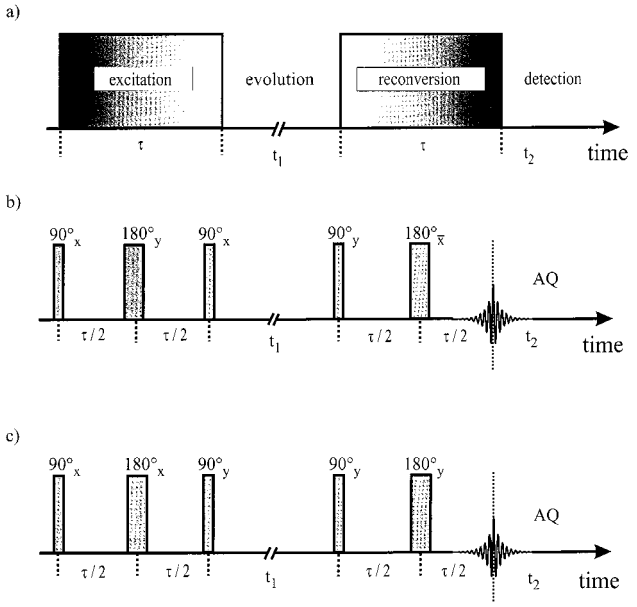

Figure 1. (a) Schematic representation of the experiment for excitation of spin multipoles in terms of dipolar encoded longitudinal magnetization and multiple-quantum coherences. This scheme is similar to that for two-dimensional MQ NMR spectroscopy, but it is used with a fixed evolution time t_1. (b) The classical three-pulse sequence supplemented by 180° refocusing pulses for measuring dipolar encoded LM and DQ filtered NMR spectra with variable excitation and reconversion times τ. The phase cycles used are different for LM and DQ experiments. (c) The three-pulse sequence supplemented with 180° refocusing pulses for TQ coherence experiments with variable excitation and reconversion times τ.

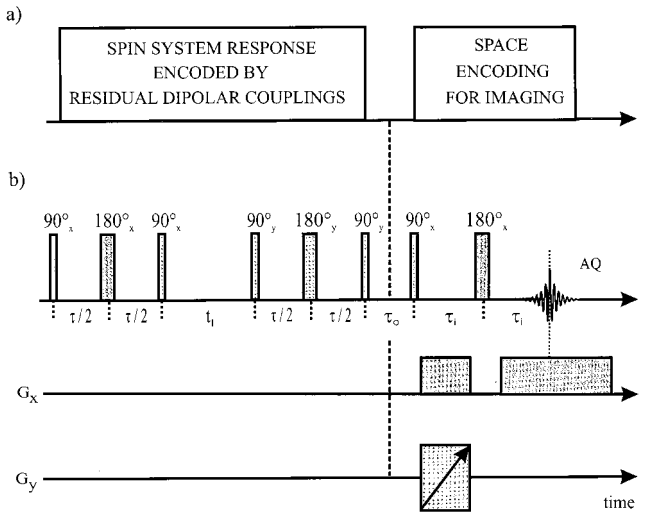

Figure 2. (a) General scheme for recording images weighted by residual dipolar couplings. (b) Three-pulse sequence with 180° refocusing pulses for filtering according to dipolar encoded LM or DQ coherences followed by a *z* filter and space encoding by two-dimensional spin-echo imaging.

was achieved by a radical mechanism. The initiator system consisted of 40% dicumyl peroxide (DCP) on kaolin as a carrier material (DICUP). For the reference PI sample the DICUP content expressed in phr (parts per hundred rubber) is 7.5. The sample was vulcanized at 150 °C until 90% of the maximum torque was achieved on the rheometer curve. Proton residual dipolar couplings extracted from the short-time regime of dipolar encoded longitudinal magnetization as well as double-quantum and triple-quantum evolution vs excitation/reconversion times provide the values $D_{\mathrm{eff}}^{\mathrm{LM}} \approx 547$ Hz, $D_{\mathrm{eff}}^{\mathrm{DQ}} \approx 1412$ Hz, and $D_{\mathrm{eff}}^{\mathrm{TQ}} \approx 220$ Hz.[30,31]

B. Measurements of ^{1}H Spin Multipoles. The measured spin multipoles include longitudinal magnetization as well as double-quantum and triple-quantum coherences and were performed at a ^{1}H frequency of 200.085 MHz on a Bruker DSX-200 spectrometer using a microimaging probe. The measurements were done at room temperature ($T = 293$ K), which corresponds to $T \approx T_g + 80$ K for the elastomers investigated. The dipolar encoded LM decays and DQ buildup intensities were recorded with the pulse sequence of Figure 1. It is based on the general scheme (cf. Figure 1a) of multiple-quantum 2D NMR spectroscopy.[34,35] The 180° radio-frequency pulses refocus the chemical shielding interaction as well as the spin interaction with the magnetic field inhomogeneities. For filtering spin multipoles phase cycling schemes were used in combination with CYCLOPS.[2] To select DQ coherences, the phases of all pulses in the excitation period were cycled in four steps of 90° increments together with a 180° phase change of the receiver phase. This phase alternation was implemented also for the DQ filtered images (see below). For dipolar encoded LM signals the receiver phase was kept unchanged. The TQ coherence buildup intensities were measured using the same pulse sequence as in Figure 1b but with a 90° phase shift of the last 90° pulse in the excitation period (cf. Figure 1c).[30] The 90° pulse length for measuring dipolar encoded LM decay curves DQ and TQ buildup curves was 2.52 μs and $t_1 = 10$ ms (LM), $t_1 = 100$ μs (DQ), and $t_1 = 50$ μs (TQ). In all experiments the excitation and reconversion times were varied in the range from 2 μs to 4.6 ms. For the spin multipole investigation, the elastic natural rubber bands were stretched using a home-built device adapted to the NMR probe that allows draw ratios $\lambda \equiv l/l_0$ up to about $\lambda = 4$, where l and l_0 are the final and initial sample lengths. The samples had a thickness of about 1 mm in the unstretched state.

C. ^{1}H NMR imaging. Proton two-dimensional (2D) LM- and DQ-filtered images encoded by the local strain were recorded with the pulse sequence shown in Figure 2. The principle of the method is based on a combination of a spin response encoded by the residual dipolar couplings and an NMR imaging technique.[2,31] The pulse sequences used for recording LM, DQ, and TQ spin multipoles (cf. Figure 1b,c) have been modified by appending a final flip-back 90° pulse. The subsequent dephasing period of duration t_0 at the end of the dipolar filter form an additional *z*-filter. The subsequent space encoding was achieved by spin-echo imaging.[1-3] The microimaging unit employed a home-built gradient coil system. The maximum achievable gradient strength was approximately 93 mT/m. The gradient was stepped through 64 gradient values. In all images the spatial resolution was about 300 μm in both directions with a field of view of about (20 mm)^2. The 90° pulse length was 33 μs. A recycle delay of 1.5 s was used in all experiments. The evolution time was fixed to $t_1 = 10$ ms and $t_1 = 100$ μs for the images recorded with the LM and the DQ filters, respectively. The filter times were set to $\tau = 0.7$ ms for the dipolar encoded LM filter and $\tau = 0.5$ ms for the DQ filter. In all cases the space encoding τ_i time was 0.8 ms. The total duration for acquisition of one filtered 2D image was on the order of 5 h.

D. Mechanical Characterization. Stress−strain measurements of the natural rubber band were performed by a Zwick 8122/500N device at a temperature of 20 °C. The measured data were fitted by the phenomenological expression

$$\sigma = \sum_{i=1}^{3} \frac{2\mu_i}{\alpha_i} (\lambda^{\alpha_i - 1} - \lambda^{-(\alpha_i/2)-1}) \qquad (1)$$

due to Ogden[36] yielding the parameters α_i and μ_i. Within experimental errors the values of these parameters agree with those reported in ref 26. A graphical representation of the stress−strain data is shown in Figure 3.

Results and Discussion

A. ^{1}H Multiple-Quantum Filtered NMR Spectra in Natural Rubber under Uniaxial Stress. The

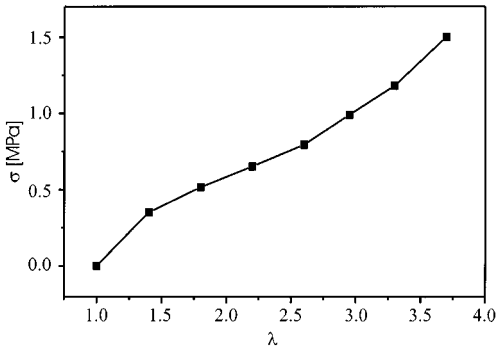

Figure 3. Stress−strain data of the natural rubber band. The solid line connecting the data points was drawn to guide the eye.

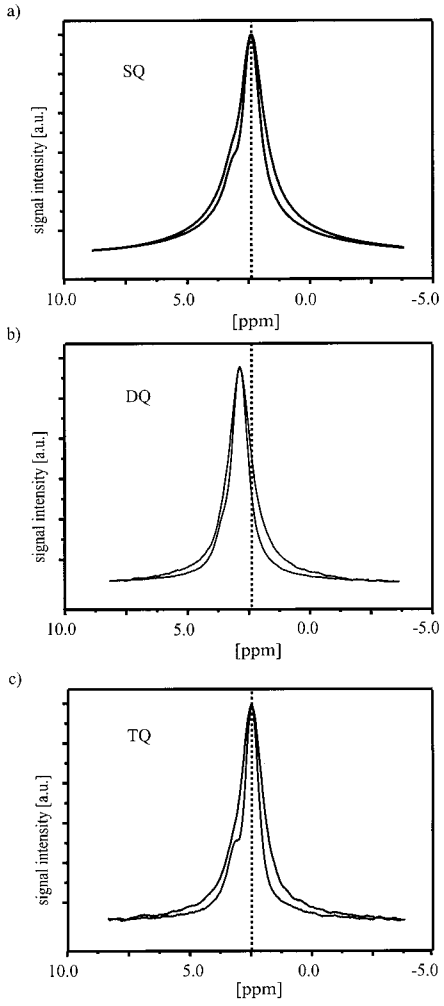

Figure 4. Filtered ^{1}H NMR spectra of a natural rubber band. Single quantum (SQ) (a), DQ (b), and TQ (c) filtered spectra are shown for an extension ratio $\lambda = 1$ (inner spectra) and for $\lambda = 3.7$ (outer spectra).

proton multiple-quantum filtered NMR spectra of natural rubber shown in Figure 4 were recorded using the pulse sequences of Figure 1b,c. The NMR absorption spectra after a single radio-frequency pulse (hereafter called single-quantum (SQ) spectra) were recorded for the relaxed ($\lambda = 1$) and the stretched ($\lambda = 3.7$) NR band (cf. Figure 4a). The proton DQ and TQ filtered NMR spectra shown in Figure 4b,c were recorded with the same values of λ as the SQ spectra.

Several features are evident from these spectra. First, all spectra are broader for $\lambda = 3.7$ compared to the relaxed state. Moreover, no line splitting is evident for the maximum draw ratio of $\lambda = 3.7$ used in this study. This fact was reported previously[37] and is different from ^{2}H spectra where a clear line splitting was measured showing a dependence governed by the $(\lambda^2 - \lambda^{-1})$ law.[38] This effect is related to the existence of a dipolar network along the polymer chain for the values of λ around unity. For larger values of λ the interchain dipolar interactions between protons have also to be taken into account. Moreover, for NR the chemical shift difference between methylene and methyl protons is small ($\delta \approx 0.5$ ppm), and the dipolar patterns produced by these functional groups start to overlap. The distribution of chemical shifts produced by conformational effects[39] will also contribute to the overall line width.

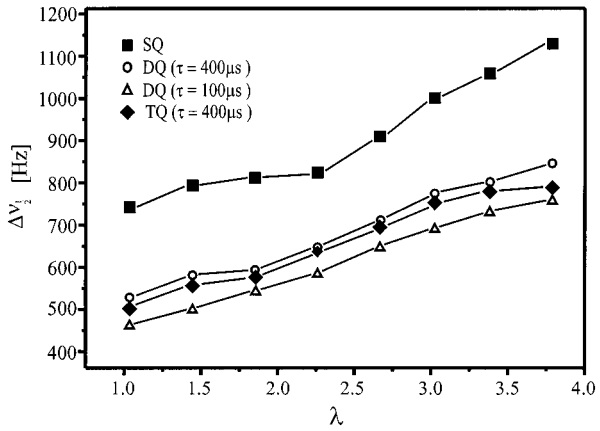

Figure 5. (a) Full width at half-height measured from SQ (squares), DQ for $\tau = 400$ μs (circles) and $\tau = 100$ μs (triangles), and TQ filtered ^{1}H NMR spectra (diamonds) vs the extension ratio λ of a natural rubber band. Straight lines are drawn through the points to indicate that the trends in the data differ for lower and larger values of the uniaxial extension.

The editing features of the DQ and TQ filtered spectra[30] are essentially preserved under moderate stretching. For the DQ case the spectrum is shifted in the methylene spectral region (cf. Figure 4b), and for the TQ edited spectrum it is shifted into the ^{1}H methyl region (cf. Figure 4c). The CH_3 group editing by the TQ filter is not perfect, and a signal from the CH functional group which contributes to the intergroup TQ coherences is also detected in the spectrum of Figure 4c for the relaxed sample. Dipolar broadening of the TQ edited spectra in the presence of mechanical stress leads to a loss of this feature (cf. Figure 4c).

B. Line Width of ^{1}H Multiple-Quantum Edited NMR Spectra under Uniaxial Stress. The full widths at half-height (fwhh) for the SQ, DQ, and TQ edited ^{1}H NMR spectra for the NR band vs the extension ratio λ are shown in Figure 5. Within the limitation of the experimental error no hysteresis effects have been detected. The fwhh for DQ and TQ edited spectra are about 60% of the fwhh of the SQ spectra for the relaxed NR sample and depend on the excitation/reconversion times τ. The presence of ^{1}H spin diffusion processes for the segmental protons is suggested by the fact that the fwhh for the DQ spectra recorded with $\tau = 100$ μs is reduced by about 20% compared to the fwhh of the DQ spectra recorded with $\tau = 400$ μs.

The dependence of the fwhh on the extension parameter λ shows the existence of two regions (cf. Figure 5). For SQ spectra, the fwhh data exhibit a steeper curve for $\lambda > 2.2$ as compared to the fwhh for $\lambda < 2.2$. The same behavior was observed for the fwhh data mea-

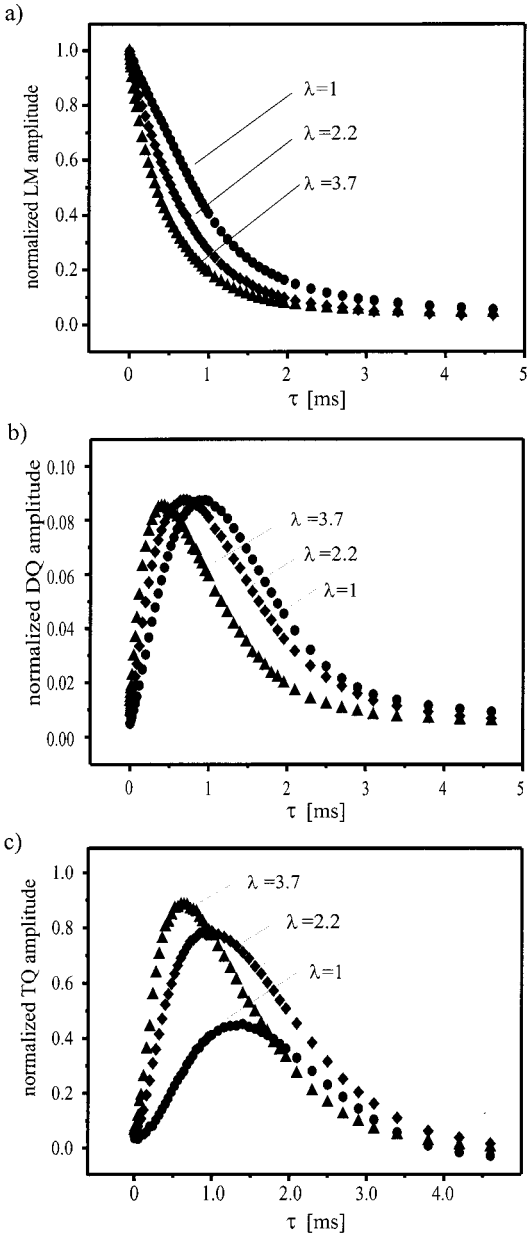

Figure 6. Proton dipolar encoded LM decay curves (a), DQ (b), and TQ (c) buildup curves of the natural rubber band recorded for different values of the extension ratio λ.

sured from DQ and TQ edited spectra, but the point of inflection is now shifted to $\lambda \approx 1.8$. This effect was reported before[37] from the measurements of the ^{1}H second van Vleck moments in NR, using a combination of spin echoes, from which a point of inflection at $\lambda \approx 1.8$ was detected. This effect can be explained by the stress-induced crystallization.[40] Moreover, the approximately linear relationship between the second moment of the orientation function obtained from Fourier-infrared measurements of the dichroism proved to be valid in the range $1 < \lambda < 4$. It is significantly enhanced with strain.[41] This proves the high segmental alignment under extension in the crystalline phase.

C. ^{1}H Residual Dipolar Couplings from the Excitation Time Dependence of the Spin Multipoles. Proton dipolar encoded LM decay curves as well as DQ and TQ buildup curves are shown in Figure 6 for the NR band with different values of the extension ratio up to $\lambda = 3.7$. The topologies of the residual dipolar couplings are edited differently by the analysis of the initial regime of the excitation/reconversion times vs τ for the different spin-multipole filters.[30] Normalized LM decay curves vs τ^2 shown in Figure 7 exibit a linear initial decay from which the square of the ^{1}H effective residual dipolar couplings $D^2_{\mathrm{LM,eff}}(\lambda)$ can be measured.[30] The DQ buildup curves (cf. Figure 6b) were fitted with a polynomial up to the sixth power in τ (not shown). From this fit the polynomial coefficient of the τ^2 term provides the effective residual dipolar coupling $D^2_{\mathrm{DQ,eff}}(\lambda)$. The normalized squares of the effective dipolar couplings, i.e., $D^2_{i,\mathrm{eff}}(\lambda)/D^2_{i,\mathrm{eff}}(1)$, where $i =$ LM and DQ are depicted in Figure 8 vs the extension parameter λ. The straight lines connecting the points reveal the existence of two distinct processes in agreement with the measurements of the fwhh (cf. Figure 5). These curves are used (see below) for obtaining stress parameter images of the stretched NR band. The theoretical prediction of the λ dependence of the $D^2_{i,\mathrm{eff}}(\lambda)/D^2_{i,\mathrm{eff}}(1)$ ratios is beyond the scope of the present work.

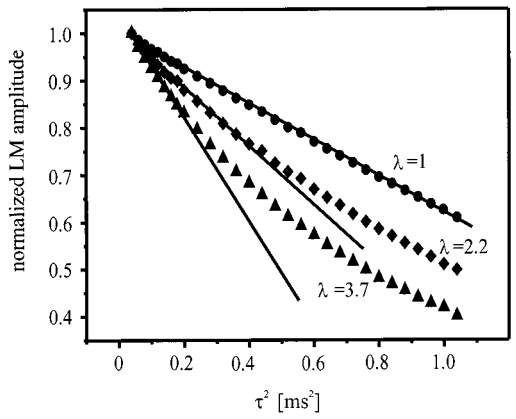

Figure 7. Initial decay of the ^{1}H dipolar encoded LM curves of Figure 6a vs τ^2 for three values of λ. The initial time behavior of the dipolar encoded LM decays exhibits a linear dependence in τ^2 (solid lines).

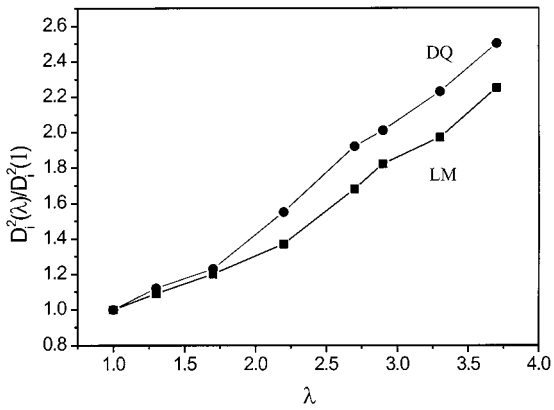

Figure 8. Ratio $D^2_{k,\mathrm{eff}}(\lambda)/D^2_{k,\mathrm{eff}}(1)$ vs extension parameter λ for $k =$ LM (squares) and $k =$ DQ (circles). Straight lines are drawn through the points to indicate that the qualitative trends in the data differ for lower and larger values of the uniaxial extension. The slopes of these curves change in the range $1.6 < \lambda < 2.2$.

D. ^{1}H NMR Mapping of Stress in Strained Elastomers. (a) Contrast Filters from Residual Dipolar Couplings. Contrast filters can be developed using the NMR techniques employed to measure the residual dipolar couplings.[31] The pulse sequence used in this work is presented in Figure 1b, where the evolution period can be chosen in the initial excitation time

regime. Dipolar encoded LM as well as DQ coherences can be employed as is demonstrated by the decay curves and buildup curves shown in Figure 6. From these figures, it is obvious that the applied filter function is highly nonlinear in the excitation/reconversion time τ. For instance, for the LM case with τ values in the initial excitation regime (cf. Figure 6a) the filtered signal decreases nonlinearly but monotonically with increasing extension ratio λ. However, a different order is followed in the case of the DQ filter if the parameter τ is set at the maximum of the buildup curves for the largest elongation λ (cf. Figure 6b). It can be seen that the signals for lower strain values decrease again nonlinearly in the λ parameter. The contrast can be inverted if the τ value is set to the signal maximum for the relaxed sample (cf. Figure 6b for $\lambda = 1$). Moreover, it is evident from the DQ buildup curves of Figure 6b that the sensitivity to the stress values is different for these τ values, being higher for the latter case. This effect is due to the fact that the DQ buildup curves are generated by the excitation of the DQ coherence in competition with high-order multiple-quantum coherences and transverse relaxation of coherences. These quantities are affected by the changes in the residual dipolar couplings as a result of increased segmental order induced by uniaxial mechanical stress.

The above results demonstrate that NMR filters based on residual dipolar couplings can be implemented for strain contrast in NMR images using dipolar encoded LM decays and DQ (or TQ (cf. Figure 6c)) coherence buildup curves. LM decays are expected to provide the highest signal-to-noise ratio and consequently the highest resolution in NMR imaging.[2] The strain contrast generated from ^{1}H residual dipolar couplings in the initial excitation time regime of LM and DQ buildup curves is about the same. The highest strain contrast can be achieved by the TQ buildup curves (cf. Figure 6c). The contrast enhancement has been shown for a TQ image of a polyisoprene phantom with a spatial distribution of cross-link density.[31] The superior contrast can be understood by considering the initial excitation time regime where the buildup rate of the TQ signal is proportional to $D^4_{\mathrm{TQ,eff}}(\lambda)$ compared to the LM and DQ filters where the rates are proportional to $D^2_{\mathrm{LM,eff}}(\lambda)$ and $D^2_{\mathrm{DQ,eff}}(\lambda)$, respectively. Nevertheless, the signal-to-noise ratio for TQ filtered NMR signals is much weaker than that for LM and DQ signals. Hence, NMR images of lower quality are obtained.[31] Therefore, only ^{1}H strain maps with LM and DQ filters are discussed below.

(b) Dipolar Encoded Longitudinal-Magnetization and Double-Quantum Filtered ^{1}H Maps of Stress. The possibility to perform ^{1}H NMR mapping of the strain distribution in elastomers was demonstrated on a natural rubber band stretched to $\lambda = 3.7$ in the direction of the main magnetic field. The band has a cut at one side. This arrangement deliberately induces an inhomogeneous strain distribution for the purpose of demonstration. Moreover, this arrangement is similar to the one used for ^{2}H NMR mapping of stress in strained natural rubber, and thus the two approaches can be directly compared.[27,28]

A two-dimensional (2D) ^{1}H image was recorded using the pulse sequences presented in Figure 2b, which consists of a residual dipolar coupling filter and spin-echo space encoding.[1−3] By suitable phase cycling either the dipolar encoded LM or DQ spin system response can be selected for contrast.[31] T_2-weighted images[1−3] were recorded using the same pulse sequence but without the contrast filters. The spatially distributed signal is given by

$$S_{\mathrm{SE}}(\vec{r};2(\tau_i+\tau)) \propto M_0(\vec{r}) \exp\left\{-\frac{2(\tau_i+\tau)}{T_2(\vec{r})}\right\} \quad (2)$$

where $M_0(\vec{r})$ is the spin density at the position $\vec{r}$ in the sample and $T_2(\vec{r})$ is the space dependent transverse relaxation time. The time interval between the 90° pulse and the spin-echo maxium is $2(\tau_i + \tau)$, where τ is the time for excitation and reconversion and $2\tau_i$ is the total echo time used for space encoding (cf. Figure 2b). The same total transverse relaxation encoding time has been assumed in the pulse sequence used for recording the images with contrast from residual dipolar couplings (cf. Figure 2b).

For the images recorded with LM and DQ contrast filters the spatially distributed signal is given by

$$S_k(\vec{r};2(\tau_i+\tau)) \propto M_0(\vec{r})\, F_k(\vec{r},D_{k,\mathrm{eff}},\tau) \times \exp\left\{-\frac{2(\tau_i+\tau)}{T_2(\vec{r})}\right\} \quad (3)$$

where k = LM or DQ depending on the detected spin multipoles, and $F_k(\vec{r},D_{k,\mathrm{eff}},\tau)$ is a spatially distributed function of the residual dipolar coupling. The residual dipolar coupling (RDC) parameter map can be obtained by correcting for the effects of spin density and transverse relaxation by dividing the filtered image by the spin-echo image. From eqs 2 and 3 we get a quotient map

$$S_k^{\mathrm{RDC}}(\vec{r};\tau) \propto F_k(\vec{r},\nabla D_{k,\mathrm{eff}},\tau) \quad (4)$$

which describes a longitudinal-magnetization (k = LM) or a double-quantum (k = DQ) residual dipolar coupling parameter map. Such a map can be quantified using different procedures. One possibility is to record various images with different values of the τ parameter equivalent to measuring spatially distributed LM decay or DQ buildup curves. In the short excitation/reconversion regime it is possible to evaluate residual dipolar couplings.[30,31] A less time-consuming method can be implemented using a homogeneous reference elastomer sample with known residual dipolar coupling for calibration. LM, DQ, and T_2-weighted images have to be recorded which show both the reference and stretched rubber band (see below). The calibration procedure can be used in the initial excitation/reconversion regime where the intensities of the signals are proportional to the square of the residual dipolar couplings.[30]

Experimental ^{1}H images recorded using LM and T_2 weights are presented in Figure 9 for a strained rubber band with a single cut at $\lambda = 3.7$ and a reference sample of cross-linked poly(isoprene). For the reference sample the residual dipolar coupling of the complex proton dipolar network has been determined from dipolar encoded LM as $D_{\mathrm{LM,eff}} \approx 547$ Hz.[30] The contrast in the LM filtered image (cf. Figure 9, top) is slightly larger than in the T_2-weighted image (cf. Figure 9, middle). Given the same total transverse relaxation time, this is a result of the influence of the residual dipolar couplings on the LM decay and the Hahn echo amplitude, bearing in mind the effect of residual dipolar

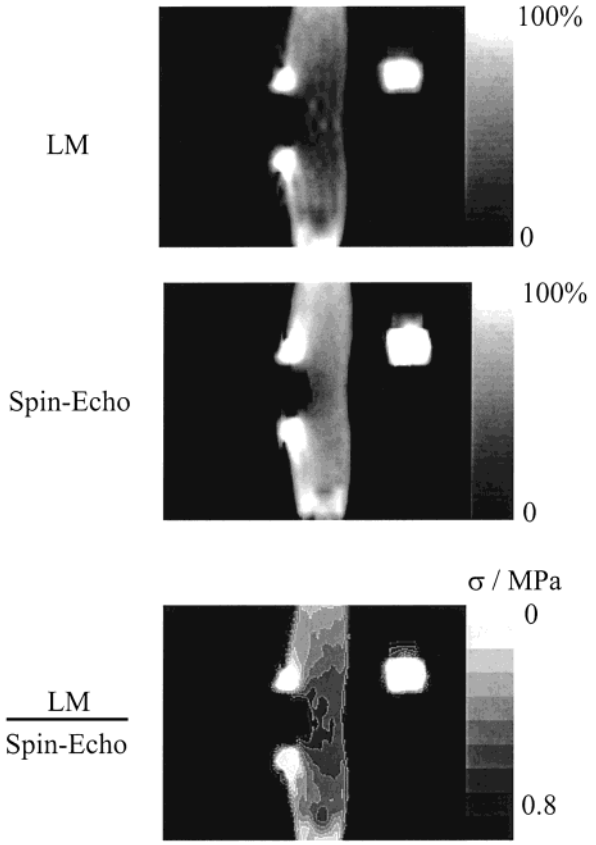

Figure 9. Two-dimensional ^{1}H NMR images of a strained natural rubber band at $\lambda = 3.7$ with a single cut weighted by residual dipolar couplings using the LM filter (top) and a spin-echo filter (middle). A stress parameter map (bottom) is obtained by forming the quotient of the LM filtered and the spin-echo images. A calibration of this map is done with the help of a reference sample of synthetic poly(isoprene) shown on the right-hand side in each image. The gray levels were reduced in the bottom map to enhance the contrast.

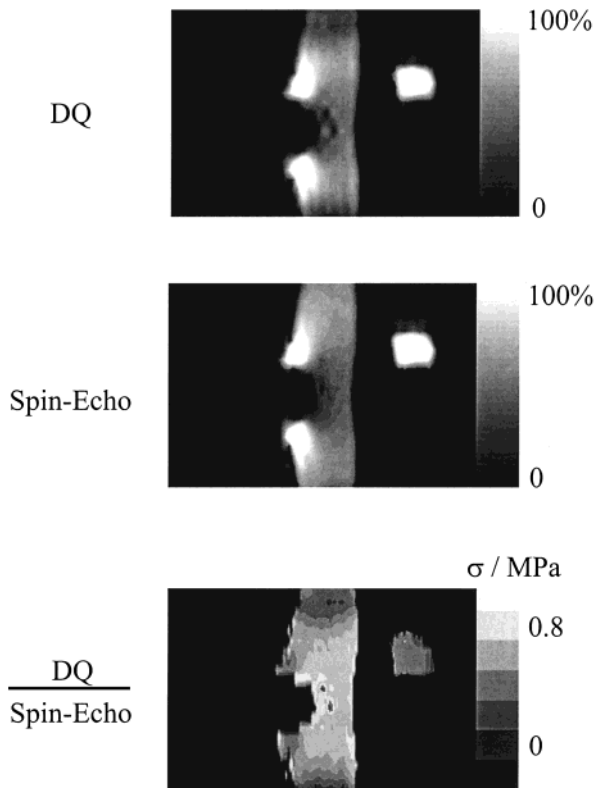

Figure 10. Two-dimensional ^{1}H NMR images of a strained natural rubber band at $\lambda = 3.7$ with a single cut weighted by residual dipolar couplings using the DQ filter (top) and a spin-echo filter (middle). A stress parameter map (bottom) is obtained by forming the quotient of the DQ filtered and the spin-echo images. A calibration of this map is done with the help of a reference sample of synthetic poly(isoprene) shown on the right-hand side in each image. To better distinguish the unstretched reference sample which should have the gray scale level corresponding to $\sigma = 0$ from the black background, we arbitrarily enhanced the intensity of this part of the map to the level corresponding to $\sigma \cong 0.4$. Moreover, the gray levels were reduced in the bottom map to enhance the contrast. The low value of the signal-to-noise ratio makes these procedures necessary.

couplings is not encoded in exactly the same way for the LM decay and the Hahn echo amplitude. The highest strain is located at the center of the cut, which is clearly represented by the signal intensities in Figure 9. Furthermore, an increase of signal intensity is exhibited in the two lips of the cut, where no increase of strain is expected on account of the sample shape. The intensity of the signal in these regions is similar to that of the relaxed poly(isoprene) reference sample. The LM quotient map is represented in Figure 9 (bottom). There, a "butterfly"-shaped distribution of strain in the areas surrounding the cut can clearly be identified. The gradient of the strain is also visible in the central region of the cut. The quotient map is a parameter map of the two-dimensional distribution of the stress parameter σ. This calibration with σ was obtained in two steps. In the first step, parameter maps (not shown) of the ^{1}H residual dipolar coupling of the strained rubber band without a cut with a small piece of synthetic poly(isoprene) as an internal reference were recorded for various extension ratios λ. The reference sample is needed in order to get the residual dipolar couplings of the strained rubber band.[30,31] In the second step the residual dipolar coupling map was converted into a stress map by using the dependence of $D^2_{LM}(\lambda)/D^2_{LM}(1)$ on the draw ratio λ from Figure 8 and the stress−strain data from Figure 3. The effective value of the residual dipolar coupling $D_{LM}(1) \approx 547$ Hz was reported in refs 30 and 31. For each value of $D^2_{LM}(\lambda)$ and corresponding stress σ a level of the gray scale was attached. An equivalent procedure would be to employ the strain dependence of the full width at the half-height of the ^{1}H spectra from Figure 5. The LM filter setting and calibration procedure allow for a semiquantitative evaluation of the stress map.

^{1}H DQ filtered image recorded with the pulse sequence of Figure 2b is shown in Figure 10 (top). The resolution is lower compared to the LM filtered image (cf. Figure 9 (top)) because the signal-to-noise ratio of the DQ signal is lower. Nevertheless, the differences between strained and relaxed regions of the cut are clearly visible. The encoding by the transverse relaxation is dominant in the image as can be seen by comparison with the spin-echo image (Figure 10, middle). If the filter weight due to the residual dipolar coupling dominated the intensities of the pixels, the region of the strained cut would show the most intense signals. In the quotient image of Figure 10 (bottom) the residual dipolar coupling weight resulting from the DQ filter defines the image contrast. Now, the most intense signals are present in the central region of the cut where the residual dipolar couplings are increased by the mechanical stress as a result of segmental orientation. The residual dipolar coupling filter was tuned in the

initial excitation time region (see Figure 6b) where for a given excitation time all buildup curves show an increase in intensity with λ. In the center of the cut a stress gradient is revealed by the map (Figure 10, bottom) in the direction perpendicular to the uniaxial stress along the rubber band. The stress contrast is reversed for the DQ parameter map compared to the LM parameter map, reflecting the use of buildup and decay curves as filters (cf. Figures 9 (bottom) and 10 (bottom)).[31] The stress parameter map recorded by the DQ filter was generated by the same procedure as that used for the LM filter (see above). For the reference sample of cross-linked poly(isoprene) the residual dipolar coupling of the complex proton dipolar network has been determined from DQ buildup curves as $D_{DQ,eff}(1) \approx 1412$ Hz.[30,31]

In principle, a TQ contrast filter can be also used for recording stress encoded maps using procedures similar to the ones discussed above. Because the TQ filtered signal is almost 2 orders of magnitude smaller than the single-quantum signal,[30] we have been unable to produce a high-quality TQ image for the strained rubber band. Nevertheless, such a ^{1}H image was reported for a phantom composed of sections of synthetic poly(isoprene) with different values of cross-link density.[31] Moreover, it was not possible to obtain a DQ gradient encoded image[2] of good quality. Nevertheless, this procedure proved to be successful for the ^{2}H DQ encoded images of deuterated poly(butadiene) oligomers incorporated into an elastic rubber band.[27,28] A possible explanation is based on the short transverse relaxation times of ^{1}H DQ coherences for a multispin dipolar topology as compared with ^{2}H DQ coherences. In the last case DQ coherence is a total spin coherence[34,35] being less sensitive to the fluctuating quadrupole interactions.

Conclusions

Measurements of ^{1}H residual dipolar couplings vs the extension ratio have been performed in a strained elastomer using NMR filters based on spin multipoles like dipolar encoded longitudinal magnetization as well as double-quantum and triple-quantum coherences. Parameters extracted from the decay and buildup curves as well as the λ dependence of the full width at half-height of the SQ, DQ, and TQ edited spectra show the existence of a stress induced crystallization process. Moreover, they are employed for calibration of the experimental data to provide stress parameter maps.

The results of this work underline the benefits of ^{1}H NMR imaging for the analysis of stress−strain effects in elastomers. The use of residual dipolar couplings of protons as a physical quantity sensitive to the segmental orientation in the presence of inhomogeneous strain distributions in elastomers has several advantages. First, the tedious synthesis of deuterated networks or the use of deuterated oligomers incorporated into the network by swelling can be circumvented. Second, the network is not modified by swelling. The potential modulation of the NMR signal encoding by the self-diffusion of the incorporated oligomers is avoided. This effect could be enhanced by the multiplicative action of the MQ coherence order on the strength of the applied field in the presence of a multiquantum evolution like in the case of ^{2}H images.[27,28] Moreover, the ^{1}H NMR detection sensitivity is much higher compared to that of ^{2}H, which substantially reduces the measuring time or improves the image resolution. In particular, the use of the dipolar encoded longitudinal magnetization filter leads to images with better contrast, compared to those obtained by ^{2}H DQ gradient encoding. Nevertheless, ^{2}H spectroscopic images can be recorded revealing quadrupole splittings and thus allowing for a strain calibration of the image pixels.[27,28] This procedure cannot be applied for the ^{1}H images recorded using the NMR lines of static samples broadened by the multispin dipolar interactions such that no line splitting can be detected. The measured ^{1}H segmental residual dipolar couplings[30] and ^{2}H quadrupole couplings[27,28] of swollen oligomers seem to be of the same order of magnitude for the investigated elastic rubber band. Thus, the sensitivity to the strain is expected to be comparable. In the initial time regime for the ^{1}H residual dipolar filters the LM and DQ parameter maps show about the same sensitivity to the local strain.

The dipolar filters discussed above can be used in combination with three-dimensional (3D) images of polymeric materials of both space distributed chemical and physical composition. Three-dimensional images of commercial polymer products revealing strong heterogeneities were reported,[42] and the contrast of these images is expected to be enhanced by the dipolar filters.

Acknowledgment. This work was supported by grants from the Bundesministerium für Bildung und Forschung (BMBF) under a German-Israeli Project Cooperation (DIP) and Deutsche Forschungsgemeinschaft (DE 780/1-1). The authors acknowledge stimulating discussion with Prof. Gil Navon, Dr. Uzi Eliav, Dr. Siegfried Stapf, and Dr. Marko Bertmer.

References and Notes

(1) Callaghan, P. T. *Principles of Nuclear Magnetic Resonance Microscopy*; Clarendon Press: Oxford, 1991.
(2) Blümich, B. *NMR Imaging of Materials*; Clarendon Press: Oxford, 2000.
(3) Kimmich, R. *NMR: Tomography, Diffusiometry, Relaxometry*; Springer-Verlag: Berlin, 1997.
(4) *Magnetic Resonance Microscopy*; Blümich, B., Kuhn, W., Eds.; VCH: Weinheim, 1992.
(5) Blümler, P.; Blümich, B.; Botto, R.; Fukushima, E. *Spatially Resolved Magnetic Resonance*; Wiley-VCH: Weinheim, 1998.
(6) Blümler, P.; Blümich, B. *NMR: Basic Princ. Prog.* **1994**, *30*, 209.
(7) Blümich, B. *Concepts Magn. Reson.* **1998**, *10*, 19; **1999**, *11*, 71; **1999**, *11*, 147.
(8) Demco, D.; Blümich, B. *Concepts Magn. Reson.* **1999**, *12*, 188; **1999**, *12*, 269.
(9) Blümich. B.; Demco, D. E. In *Spectroscopy of Rubbery Materials*; De, P. P., Litvinov, V. E., Eds.; Shrewsbury: Rapra, 2001.
(10) Demco, D. E.; Hafner, S.; Spiess, H. W. In *Spectroscopy of Rubbery Materials*; De, P. P., Litvinov, V. E., Eds.; Shrewsbury: Rapra, 2001.
(11) Blümler, P.; Blümich, B. *Rubber Chem. Technol.* **1997**, *70*, 468.
(12) Blümler, P.; Blümich, B. *Macromolecules* **1991**, *24*, 2183.
(13) Spyros, A.; Chandarkumar, N.; Heidenreich, M.; Kimmich, R. *Macromolecules* **1998**, *31*, 3021.
(14) Chudek, J. A.; Hunter, G. *J. Mater. Sci., Lett.* **1992**, *11*, 222.
(15) Hafner, S.; Barth, P. *Magn. Reson. Imaging* **1995**, *5*, 739.
(16) Spyros, A.; Kimmich, R.; Briese, B. H.; Jendrossek, D. *Macromolecules* **1997**, *30*, 8278.
(17) Fyfe, C. A.; Randall, L. H.; Burlinson, N. E. *J. Polym. Sci., Part A: Polym. Chem.* **1996**, *31*, 159.
(18) Hafner, S.; Kuhn, W. *Magn. Reson. Imaging* **1994**, *12*, 1075.
(19) Sarkar, S.; Komoroski, R. A. *Macromolecules* **1992**, *25*, 1420.
(20) Chang, C.; Komoroski, R. A. *Macromolecules* **1989**, *22*, 600.

(21) Garrido, L.; Mark, J. E.; Sun, C. C.; Ackerman, J. L.; Chang, C. *Macromolecules* **1991**, *24*, 4067.
(22) Smith, S. R.; Koenig, J. L. *Macromolecules* **1991**, *24*, 3496.
(23) Kuhn, W.; Barth, P.; Hafner, S.; Simon, G.; Schneider, H. *Macromolecules* **1994**, *27*, 5773.
(24) Barth, P.; Hafner, S.; Denner, P. *Macromolecules* **1996**, *29*, 1655.
(25) Günther, E.; Blümich, B.; Spiess, H. W. *Macromolecules* **1992**, *25*, 3315.
(26) Blümler, P.; Blümich, B. *Acta Polym.* **1993**, *44*, 125.
(27) Klinkenberg, M.; Blümler, P.; Blümich, B. *Macromolecules* **1997**, *30*, 1038.
(28) Klinkenberg, M.; Blümler, P.; Blümich, B. *J. Magn. Reson.* **1996**, *A 119*, 197.
(29) Graf, R.; Demco, D. E.; Hafner, S.; Spiess, H. W. *Solid State Nucl. Magn. Reson.* **1998**, *12*, 139.
(30) . Schneider, M.; Gasper, L.; Demco, D. E.; Blümich, B. *J. Chem. Phys.* **1999**, *111*, 402.
(31) Schneider, M.; Demco, D. E.; Blümich, B. *J. Magn. Reson.* **1999**, *140*, 432.
(32) Tsoref, L.; Shinar, H.; Seo, Y.; Eliav, U.; Navon, G. *Magn. Reson. Med.* **1998**, *39*, 11.
(33) Seo, Y.; Ikoma, K.; Takamiya, H.; Kusaka, H.; Tsoref, L.; Eliav, U.; Shinar, H.; Navon, G. *Magn. Reson. Med.* **1999**, *42*, 884.
(34) Ernst, R. R.; Bodenhausen, G.; Wokaun, A. *Principles of Nuclear Magnetic Resonance in One and Two Dimensions*; Clarendon: Oxford, 1987.
(35) Munowitz, M.; Pines, A. *Adv. Chem. Phys.* **1987**, *66*, 2.
(36) Ogden, R. W. *Proc. R. Soc. London* **1972**, *A326*, 565.
(37) Warner, M.; Callaghan, P. T.; Samulski, E. T. *Macromolecules* **1997**, *30*, 4733.
(38) Sotta, P.; Deloche, B.; Herz, J.; Lapp, A.; Durand, D.; Rabadeux, J. C. *Macromolecules* **1987**, *20*, 2769.
(39) Schmidt-Rohr, K.; Spiess, H. W. *Multidimensional Solid-State NMR and Polymers*; Academic Press: London, 1994.
(40) Erman, B.; Mark, J. E. *Structures and Properties of Rubber-like Networks*; Oxford University Press: New York, 1997.
(41) Amram, B.; Bokobza, L.; Queslel, J. P.; Monnerie, L. *Polymer* **1986**, *27*, 877.
(42) Kennedy, C. B.; Balcom, B. J.; Mastikhin, I. V. *Can. J. Phys.* **1998**, *76*, 1753.

MA001983N